



Full Length Article

Near-wall dynamics of premixed methane/air flames

Jian Zhu^a, Jianfeng Pan^{a,*}, Feichi Zhang^{b,c}, Thorsten Zirwes^{b,d}, Abiodun Oluwaleke Ojo^a, Feiyang Li^a

^a School of Energy and Power Engineering, Jiangsu University, Zhenjiang 212013, PR China

^b Engler-Bunte-Institute, Division of Combustion Technology, Karlsruhe Institute of Technology, Engler-Bunte-Ring 1, 76131 Karlsruhe, Germany

^c Institute for Technical Chemistry, Karlsruhe Institute of Technology, Hermann-von-Helmholtz-Platz 1, 76344 Eggenstein-Leopoldshafen, Germany

^d Steinbuch Centre for Computing (SCC), Karlsruhe Institute of Technology, Hermann-von-Helmholtz-Platz 1, Karlsruhe, Germany



ARTICLE INFO

Keywords:

Flame stretch
Flame dynamics
Flame wall interaction
Unsteady FWI
OpenFOAM

ABSTRACT

This work focuses on sidewall quenching (SWQ) for premixed methane/air flames that are forced by a periodic oscillatory inflow with excitation frequency $f = 100$ Hz. The effects of steady-state and transient flame stretch on the near-wall flame dynamics are evaluated using two-dimensional direct numerical simulation (2D-DNS) and the GRI 3.0 reaction mechanism. The velocity fluctuations lead to significant changes in flame speed and flame stretch, as well as the associated Markstein numbers. The phenomenon of SWQ is analyzed using flame quenching distance, wall heat flux and heat release rate. For steady-state conditions, there is a strong correlation between the maximum wall heat flux (WHF_{max}) and the flame quenching Peclet Number (Pe_q), as well as between the flame speed and the flame stretch; for transient conditions, the flame quenching distance (d_q) increases continuously from phase angles of $1/4f^{-1}$ to $3/4f^{-1}$ in one cycle as time progresses, and the fluctuation of the quenching distance (Δd_q) decreases gradually with increasing equivalence ratio (ϕ). The flame stretch changes from negative to positive in the process from $1/4f^{-1}$ to $3/4f^{-1}$, while the heat release rate and fuel reaction rate near the wall gradually decrease. Furthermore, the FWI region is dominated by negative flame stretch while positive flame stretch is present at the base of the flame. Moreover, the methane/air flame has a nearly twofold increase in the consumption speed during the oscillation from phase angle $3/4f^{-1}$ to the next cycle at $1/4f^{-1}$ at $\phi = 0.5$ and $\phi = 1.0$. These results show that flow field perturbations are not negligible in elucidating the effects of flame-wall interactions.

1. Introduction

Flame-wall interaction (FWI) describes the two-way coupling process between the flame and a wall, which is an active research topic. The phenomenon is important to the operation and design of many closed combustion systems, including internal combustion engines and aero engines. The impact of FWI is enhanced by the increase of surface to volume ratio when the combustor size is reduced. The heat loss of the flame to the wall often causes local thermal stress, local quenching and reburning, and unburnt hydrocarbon emissions. As a result, a better understanding of the behavior of flames near the wall and the influence of FWI on the combustor performance is a topic of interest.

The impact of wall heat loss on flammability and instability during flame-wall interaction has been the subject of numerous studies. According to Kim et al. [1], the quenching behavior may be broken down into three temperature ranges: quenching at wall temperatures between

100 and 350 °C, driven by wall heat loss; quenching between 400 and 600 °C, determined by heterogeneous chemical reactions of surface radicals, with the quenching distance increasing with increasing surface temperature; and quenching beyond 600 °C, where the homogeneous reactions overcome radical desorption and the flame is more difficult to extinguish. By accurately regulating the wall temperature and measuring the flame temperature and near-wall radical concentration quantitatively, Fan et al. [2] investigated the flame-wall coupling process in a microscale combustor. It was discovered that the quenching distance of the heated quartz wall could be less than 0.7 mm, and that the size of the quenching distance depends on the wall temperature. With the aid of PLIF and PIV, Jainski et al. [3–4] investigated the sidewall quenching (SWQ) phenomenon of a turbulent V-shaped flame from a Bunsen burner. Using two different methods to determine the quenching distance of the flame, they analyzed the near-wall behavior of the flame consumption rate and compared it with the behavior of a freely propagating laminar flame. In addition, they showed that the

* Corresponding author.

E-mail address: mike@ujs.edu.cn (J. Pan).

<https://doi.org/10.1016/j.fuel.2022.125774>

Received 29 April 2022; Received in revised form 18 August 2022; Accepted 21 August 2022

Available online 12 September 2022

0016-2361/© 2022 Elsevier Ltd. All rights reserved.

Nomenclature			
a	Amplitude	θ	Angle between the tangential direction of the flame surface and the wall surface
CFL	Courant-Friedrichs-Lewy number	Pe_q	Flame quenching Peclet Number
CARS	Coherent anti-Stokes Raman Spectroscopy	PLIF	Planar Laser Induced Fluorescence
d_q	Flame quenching distance	PIV	Particle Image Velocimetry
Δd_q	Fluctuation of the quenching distance	\dot{q}_r	Heat release rate
DNS	Direct numerical simulation	\dot{q}_{rmax}	Maximum heat release rate
D	Diffusion coefficient of the species	s	Flame surface segment length
EGR	Exhaust Gas re-circulation	S_c	Flame consumption speed
f	Excitation frequency	S_L^0	1D laminar flame speed
FWI	Flame wall interaction	S_d	Flame displacement speed
\hat{h}_k^0	Standard heat of formation of species k	SWQ	Sidewall quenching
HOQ	Head-on quenching	T_{iso}	Isotherm
k	Heat conductivity of the unburnt gas	T_w	Wall temperature
κ	Flame curvature	$u(x)$	Parabolic velocity profile for the steady-state
K	Flame stretch	\vec{u}	Flow field velocity
Ka	Karlovitz number	u_{in}	Maximum inflow velocity
Ka_s	Non-dimensional aerodynamic strain	$u_{in}(x,t)$	Parabolic velocity profile for the transient cases
K_s	Flame aerodynamic strain	w_q	Profile width (w_q) at the peak of WHF 10 %
Ka_c	Non-dimensional stretch due to curvature	WHF	Wall heat flux
K_c	Flame stretch due to curvature	WHF_{max}	Maximum wall heat flux
L_a	Markstein length	Y_{rmax}	Maximum fuel consumption rate
Le	Lewis Number	δ_{th}	Flame thickness
Ma	Markstein number	$\dot{\omega}_F$	Fuel reaction rate
\vec{n}	Flame surface normal vector	δ_L^0	1D laminar flame thickness
α	Thermal diffusivity of the reactant mixture	ϕ	Equivalence ratio

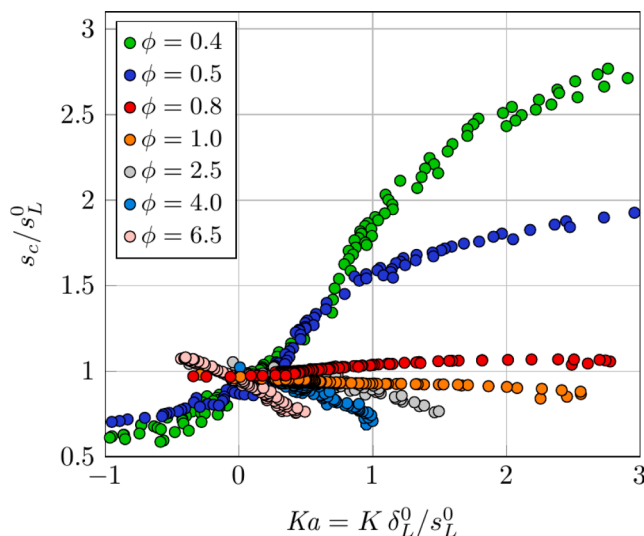


Fig. 1. Correlation of laminar flame speed S_c over normalized stretch Ka for hydrogen/air Bunsen flames, adapted from [18].

influence of the wall caused the fuel reaction rate to be much lower near the wall and the flame front to re-laminarize. Chen et al. [5] looked into how the sidewall tilt angle and inlet gas parameters affected the flame structure and combustion limit with/without the side wall. The suppression impact of a sidewall on flame stretching downstream is reinforced as the Reynolds number increases, but it was greatly reduced as inlet gas temperature increased. Yang et al. [6] discovered that the quenching distance of the combustor varies with different wall materials. The aforementioned studies analyzed flame quenching events and the trend of the wall heat flux using experimental techniques. Other scholars considered numerical simulation methods as an effective

research tool. According to De Lataillade et al. [7], wall heat flux increases in a diffusion burner as the flame approaches the wall and is higher for diffusion flames than for premixed flames under the same operating conditions. Popp et al. [8] performed a numerical analysis of the head-on quenching (HOQ) of methane/air and propane/air flames. When the wall temperature rises, the wall heat flux increases and the concentration of free radicals in the near-wall region becomes higher. Therefore, surface reactions, such as adsorption and desorption of free radicals, should also be taken into account, and the importance of thermal diffusion cannot be neglected. The FWI for laminar hydrogen-oxygen combustion was studied by Dabireau et al. [9] using direct numerical simulation (DNS), comparing the maximum wall heat flux and the duration of the FWI between premixed and diffusion combustion. They discovered that although the diffusion flame had a lower wall heat flux but a longer residence time with high wall heat flux, the premixed flame had a greater wall heat flux but a shorter residence time before quenching. Yenerdag et al. [10] looked at how heat loss and quenching distance were affected by EGR, equivalence ratio, initial pressure, and wall temperature. They found that the change in EGR in the fuel mixture has a significant impact on both the maximum wall heat flux and the heat flux caused by the temperature of the burnt gas. The corresponding homogeneous wall reaction rates on the wall boundaries were studied by Strassacker et al. [11] using the REDIM calculation method. Jafarholi et al. [12] conducted a quantitative analytical study of the quenching distance, wall heat flux distribution and wall heat transfer process of laminar premixed flames in a flat plate burner and found that the thickness of the flame was halved due to increased pressure and unstable heat diffusion.

Flame stretch rate is a crucial covariate determining the flame dynamics [13–21] and is of great analytical value for the investigation of FWI. Law [13] showed that the various effects caused by flame curvature, flow field inhomogeneities, and flame instability can be described by the flame stretch rate. According to Creta et al. [14], the strain rate can have an additional stabilizing effect during the nonlinear evolution of an unstable flame, delaying the onset of hydrodynamic instability.

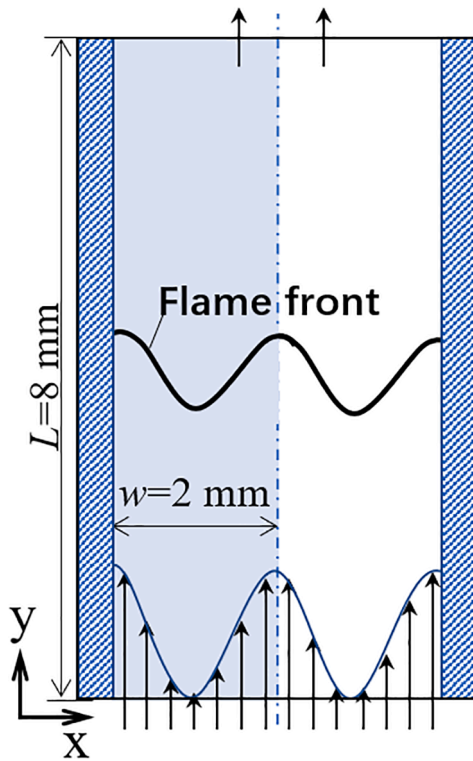


Fig. 2. Dimensions of the computational domain.

Liang et al. [15] proposed a finite thickness expression not only to facilitate the extraction of laminar flame speeds, but also to indirectly obtain the thickness and Markstein length of the laminar flame. Gianakopoulos et al. [16] studied weakly stretched flames and established that, according to asymptotic theory, both flame displacement speed and flame consumption speed are linearly proportional to flame stretch for various Markstein lengths. Zhang and Chen et al. [17–19] compared the impact of the presence/absence of a wall surface on the flame and found that the flame approaching a cold wall is compressed by the slower flow near the wall, which causes the FWI to be dominated by negative flame stretch; in contrast, for freely propagating flames, the elongation process is a shift from positive tangential stretch to negative tangential stretch, as depicted in Fig. 1. Additionally, it was discovered that a linear relationship between the flame speed and the normalized total stretch held true only for low stretch values, as seen in Fig. 1. Furthermore, it is challenging to overcome the impact of unstable perturbations on flame combustion properties in practical applications. According to Zirwes et al. [20], fluctuations in flame height have been implicitly accounted for in the OH-LIF and CARS data, and the quenching distances derived from free radical OH and CH by capturing the temporal average of experimental measurements can be overestimated. Palulli et al. [21] analyzed flame dynamics and CO emission patterns of methane/air preheated oscillating flames under these conditions and found that approximately 50 % of the total heat release rate would be transferred to the wall at the moment of quenching. Analysis of CO species transport showed that it was dominated by convection and diffusion when approaching the wall towards the top of the flame.

It is obvious that the flame structure and combustion properties in the FWI zone are significantly influenced by wall heat loss and flame stretch. As a result, several researchers examined how changing wall temperatures and wall materials affect flame quenching behavior and discovered that wall effects also greatly altered flame stretch. Less research has examined the phenomenon of unsteady flame fluctuations caused by inflow perturbations on FWI, and very few of the studies mentioned above have been analyzed in conjunction with wall heat loss and its impact on flame stretch. Methane is chosen as fuel in study

because it is frequently utilized in gas turbines and because the preheated mixture and the wall is comparable to those seen at the combustor inlet of turbines. Using crucial parameters like quenching distance, wall heat flux, and flame heat release rate, direct numerical simulations are performed to characterize the flame-wall interaction behavior under forced oscillating inflow conditions. The focus is laid on the change in flame structure during transient flame-wall interaction in terms of flame consumption speed and flame stretch rate.

2. Theoretical basics

2.1. Flame stretch

Karlovitz [22] considered flame stretch as the main factor affecting the local flame dynamics and as the main parameter controlling the flame structure. Flame stretch (K) is defined by Eq. (1.1) as the logarithmic Lagrangian time derivative of the area A of an element on the flame surface [23]:

$$K \equiv \frac{1}{A} \frac{dA}{dt} \quad (1.1)$$

Often, it is more practical to rewrite the expression for flame stretch in the following equivalent way [24]:

$$K = -\vec{n} \cdot \vec{n} : \nabla(\vec{u} + S_d \vec{n}) + \nabla \cdot (\vec{u} + S_d \vec{n}) \quad (1.2)$$

The first term on the right hand side of Eq. (1.2) represents the rate of stretch perpendicular to the flame surface, and the second term the stretch in the normal direction. \vec{n} denotes the flame surface normal vector and points toward the unburnt gas; \vec{u} is the flow field velocity; S_d is the displacement speed of the flame, here evaluated at the flame surface defined by the fuel mass fraction corresponding to the position of maximum reaction rate in an unstretched flame $Y_F = Y_{Fmax}$.

$$S_d = -\frac{1}{|\nabla Y_F|} \frac{dY_F}{dt} = -\frac{\dot{\omega}_F + \nabla \cdot (\rho D_F \nabla Y_F)}{\rho |\nabla Y_F|} \quad (1.3)$$

where $\dot{\omega}_F$ is the reaction rate of fuel, ρ the density and D_F the diffusion coefficient of the fuel species; $\vec{u} + S_d \vec{n}$ is the absolute movement velocity of the flame front.

The contributions to flame stretch from Eq. (1.2) can be reorganized as follows:

$$K = -\vec{n} \cdot \vec{n} : \nabla \vec{u} + \nabla \cdot \vec{u} - \vec{n} \cdot \vec{n} : \nabla S_d \vec{n} + \nabla \cdot S_d \vec{n} \quad (1.4)$$

In Eq. (1.4), $-\vec{n} \cdot \vec{n} : \nabla \vec{u} + \nabla \cdot \vec{u} = K_s$ indicates the aerodynamic strain; $-\vec{n} \cdot \vec{n} : \nabla S_d \vec{n} + \nabla \cdot S_d \vec{n} = S_d \kappa = K_c$ is the flame stretch due to a curved, propagating flame, with $\kappa = \nabla \cdot \vec{n}$ the flame curvature.

The local Karlovitz number (Ka) is the normalized local flame stretch K . It therefore describes flame bending and flame displacement under various forms of stretch caused by inhomogeneities in the internal flow field. It is defined as $Ka = K \delta_L^0 / S_L^0 = Ka_s + Ka_c$, which consists of two parts, the aerodynamic strain (Ka_s) and the flame curvature strain (Ka_c).

2.2. Flame consumption speed (S_c)

The local flame speed is computed from the rate of the consumption of the fuel species [25]:

$$S_c \equiv -\frac{1}{\rho^u (Y_F^u - Y_F^b)} \int_{-\infty}^{+\infty} \dot{\omega}_F dn \quad (1.5)$$

where $\dot{\omega}_F$ denotes the fuel reaction rate; dn is the direction perpendicular to the flame surface. Since flame speed is calculated by integration of the reaction rate at each point along the normal coordinate of the flame surface, each point on the flame front has a corresponding flame speed that is largely insensitive to the choice of flame isosurface [25]. Therefore, S_c is to some extent more robust than the displacement speed. The

Table 1
Calculated results of 1D unstretched methane/air flames ($T_u = 773$ K).

ϕ [-]	0.5	0.8	1.0	1.3
S_L^0 [m/s]	0.950	1.940	2.194	1.790
δ_L^0 [mm]	0.477	0.311	0.287	0.316
T_{iso} [K]	1480 K	1680 K	1820 K	1850 K
Y_{rmax} [-]	0.003547	0.006427	0.008317	0.010841
Le [-]	0.972	0.970	0.969	0.968

integral result in Eq. (1.5) is always greater than or equal to zero, as the reaction rate of fuel is mostly negative, and it approaches zero at the position where the flame is quenched and no combustion reaction occurs.

3. Numerical formulation

3.1. Simulation setups

The computational setup is shown in Fig. 2: the light blue area is the computational domain, and its dimension is $L \times w = 8 \times 2$ mm²; the left boundary is defined as an isothermal wall with the same temperature ($T_w = T_u$) as that of the fresh gas. The right boundary of the computational domain (vertical centerline in Fig. 2) is set as symmetry. Consequently, an assumption of an inert wall, consistent with [17,18,20], is applied. The inlet uses a parabolic velocity profile with a minimum velocity of zero as provided by the Poiseuille solution [27], as seen in Fig. 2. The inlet velocity function given by $u(x) = u_{in} [1 - x^2/(w/2)^2] = u_{in} (1 - 4x^2/w^2)$ leads to a V-shaped flame which is convenient for studying the flame tip near the wall. The no-slip boundary condition for the wall together with the prescribed non-zero velocity at the wall at the inlet leads to the development of a boundary layer in the vicinity of the high velocity region. The flame is stabilized inside the computational domain by adjusting the bulk velocity. The flow in the near-wall region is intrinsically laminar due to the non-slip condition, which allows the flame to be stabilized at a relatively low propagation speed, which is of the order of S_L^0 [30]. Lean flames ($\phi = 0.5$; $\phi = 0.8$), stoichiometric flame ($\phi = 1$) and a rich flame ($\phi = 1.3$) are selected for this study, with the calculated flame parameters of the corresponding 1D unstretched freely propagating flames listed in Table 1. ϕ is the equivalence ratio of the methane/air flames; u_{in} is the maximum flow velocity in the parabolic inlet profile; S_L^0 is the 1D flame laminar speed of the unstretched flame. Premixed methane/air flames in a combustor with a wall temperature

(T_w) of 773 K and a pressure (P_0) of 1 bar are used. The fresh gas enters the combustor along the y-axis and the preheated mixture temperature (T_0) is set to 773 K. Table 1 also presents δ_L^0 , which denotes the 1D laminar flame thickness and is calculated from:

$$\delta_L^0 = \frac{\max(T) - \min(T)}{\max(|\frac{\partial T}{\partial n}|)} \quad (1.6)$$

where $\partial T/\partial n$ denotes the temperature gradient in the flame normal direction; Y_{rmax} is the maximum fuel consumption rate for the unstretched flame. The flame isosurface used for the following analysis is defined by the isosurface of Y_{rmax} [12]. A second definition for the flame surface in this work uses an isosurface of temperature (T_{iso}) as the flame surface which is obtained from the temperature corresponding to the maximum heat release rate gradient in the unstretched flame [25]. The positions of the flame surface obtained by the two methods are very close to each other, and the difference in the methods lies in the flame surface distribution near the wall (zero-gradient for species mass fractions at the wall vs fixed value for the temperature). $Le = \alpha/D$ is the Lewis number. It describes the magnitude of heat and mass transfer and is an important parameter to measure the effect of stretch on the flame; α and D denote the thermal diffusivity and the diffusion coefficient of the reactant mixture.

The computational domain is discretized into a sufficiently refined grid with a cell size of 20 μ m, and the flame thickness (δ_{th}) is resolved by at least 10 to 17 cells to ensure accurate results. The maximum Courant-Friedrichs-Lewy number (CFL) and Fourier number are 0.2 and 0.35.

The DNS solver from [29] is used, which is based on an in-house extension of OpenFOAM [32,33]. The GRI 3.0 reaction mechanisms is used to compute chemical reaction rates. Molecular diffusion is considered with the mixture-averaged transport model (Curtiss-Hirschfelder approximation), taking into account differential diffusion. The compressible Navier-Stokes equations are solved with the finite volume method based on the assumption of an ideal gas, including mass conservation, species mass fractions and energy conservation [25]. A second-order fully implicit time discretization and a fourth-order spatial interpolation scheme are used to discretize spatial derivatives. The open-source libraries Cantera [34] and Sundials [26] are used to provide detailed diffusion coefficients and efficient routines for computing the chemical source terms. The correctness of the DNS solver has been demonstrated and detailed description along with validations can be found in [29–31].

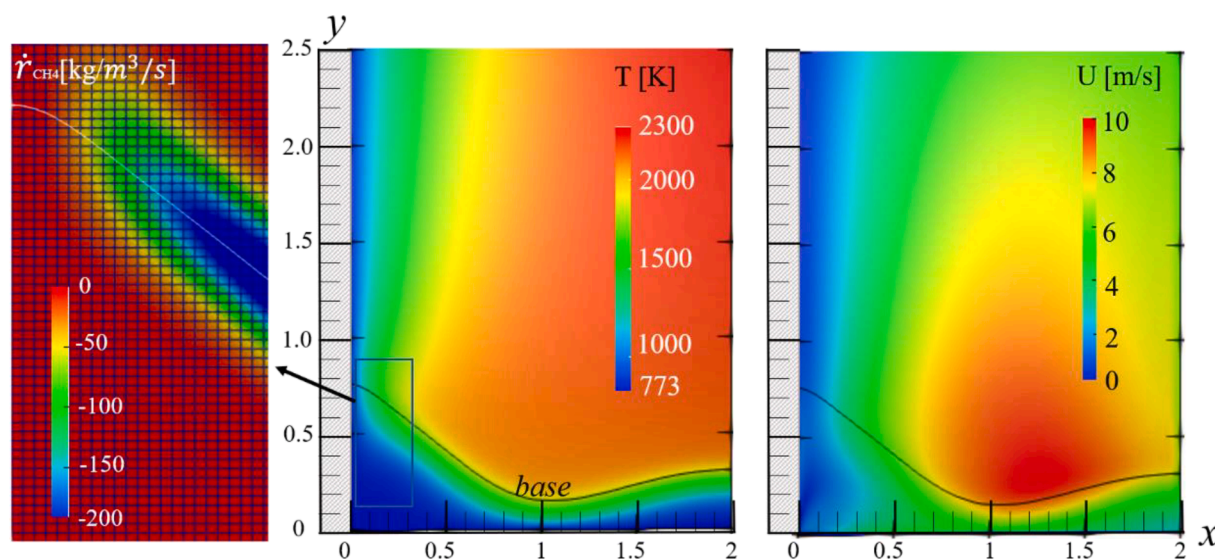


Fig. 3. Contours of local consumption rate (\dot{r}_{CH_4}), temperature (T), and velocity (U) for a stoichiometric flame ($\phi = 1$). Dimensions along the x and y axis in mm.

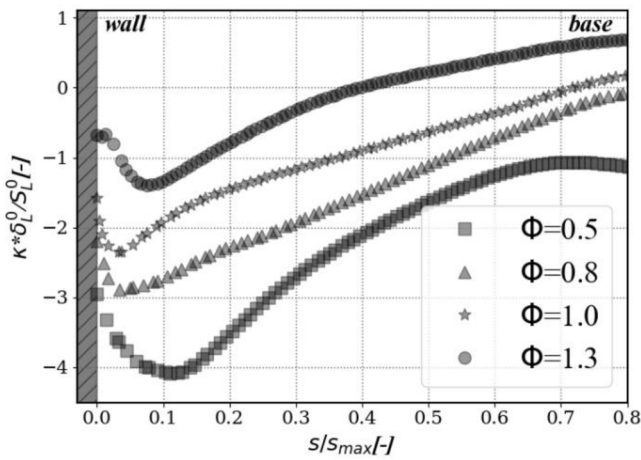


Fig. 4. Magnitude of the stretch rate along the flame surface for different equivalence ratios.

3.2. Numerical setup

Fig. 3 shows the contours of the temperature (center) and velocity (right) for a stoichiometric flame, where the flame surface is given by the solid black line. It shows the location of the flame with the isoline of Y_{rmax} , in which the flame is located relatively far downstream near the wall. The wall is at the $x = 0$ mm location, while the flame base is close to the $x = 1$ mm point. The figure on the left displays the contours of the local consumption rate \dot{r}_{CH_4} of the fuel, along with the grid lines and the equivalent surface $Y_{CH_4} = Y_{rmax}$ (white solid line). The reaction zone with $\dot{r}_{CH_4} < 0$ is fully resolved in the near-wall region, and the maximum wall distance found at the FWI location is calculated as $x^+ = 0.28$, which justifies the used grid resolution.

4. Results and analysis

4.1. Steady-state flames

The steady-state FWI analysis was performed using the 1D laminar flame characteristics indicated in Table 1 for the lean flames ($\varnothing = 0.5$; $\varnothing = 0.8$), stoichiometric flame ($\varnothing = 1$) and rich flame ($\varnothing = 1.3$), respectively. u_{in} is always equal to S_L^0 for the different equivalence ratios. The wall temperature is equal to the fluid temperature, $T_w = T_u = 773$ K, and pressure, $P_0 = 1$ atm, which are associated with gas turbine inlet conditions. The study of the weakly curved part of the flames ($Ka_c \approx 0$) is

the main subject of this section, excluding the impact of flame normal stretch due to curvature.

Fig. 4 illustrates the trend of the aerodynamic strain along the flame surface for various equivalence ratios. The horizontal axis indicating the tangential coordinate s/s_{max} along the flame surface and the vertical axis indicating the normalized stretch rate $K\delta_L^0/S_L^0 = Ka$ which is also equal to the aerodynamic strain (Ka_c) assuming low curvature. In the near wall region ($s/s_{max} < 0.1$), the flow velocity is reduced, and the compressive strain leads to more negative stretch. In addition, the temperature difference between the wall and the flame creates thermal convection which also affects the internal flow. For the region away from the wall ($s/s_{max} > 0.1$), Ka begins to rise from -4.1 to 0.9 along the flame surface and reaches its peak at the flame base. This phenomenon is exactly opposite to the trend of the freely propagation flame stretch rate, in which aerodynamic strain continuously decreases until it reaches zero [17]. The present findings demonstrate that this phenomenon can be extended to high temperature isothermal wall and small-scale conditions. Moreover, Ka along the flame surface in the near-wall region is most pronounced at $\varnothing = 0.5$, followed by $\varnothing = 1.0$, $\varnothing = 0.8$, and finally $\varnothing = 1.3$. This trend is due to the larger methane fuel mass fraction gradient near the wall.

For various equivalence ratios, the distribution of the wall heat flux (WHF) versus the heat release rate (\dot{q}_r) along the y -axis near the wall is shown in Fig. 5. The heat release rate (\dot{q}_r) is calculated from $\dot{q}_r = -\sum_k h_k^o \dot{\omega}_k$, where h_k^o denotes the standard enthalpies of formation of the chemical species. WHF and \dot{q}_r both exhibit similar trends regarding the position of the respective peaks. When WHF reaches its maximum value, the flame quenching distance reaches the minimum and, due to the heat loss to the wall, \dot{q}_r also decreases. The flame quenching distance (d_q) is defined as the distance from the quenching point to the wall and the point on the isotherm closest to the wall. According to the aforementioned operating conditions, d_q is 0.44 mm, 0.28 mm, 0.25 mm, and 0.36 mm, respectively.

Poinsot [37] also proposed a correlation between the maximum wall heat flux (WHF_{max}) and the quenching Peclet number (Pe_q) with the following expression.

$$WHF_{max} = \frac{T_{ad} - T_{wall}}{T_{ad} - T_u} \frac{1}{Pe_q} \quad (1.7)$$

where, at a minimal Peclet number known as the quenching Peclet number, Pe_q , quenching takes place. It can be written as $Pe_q = d_q/\delta_L^0$ and is defined as the quenching distance normalized by the premixed flame thickness δ_L^0 .

Here, the wall temperature is equal to the temperature of fresh gas

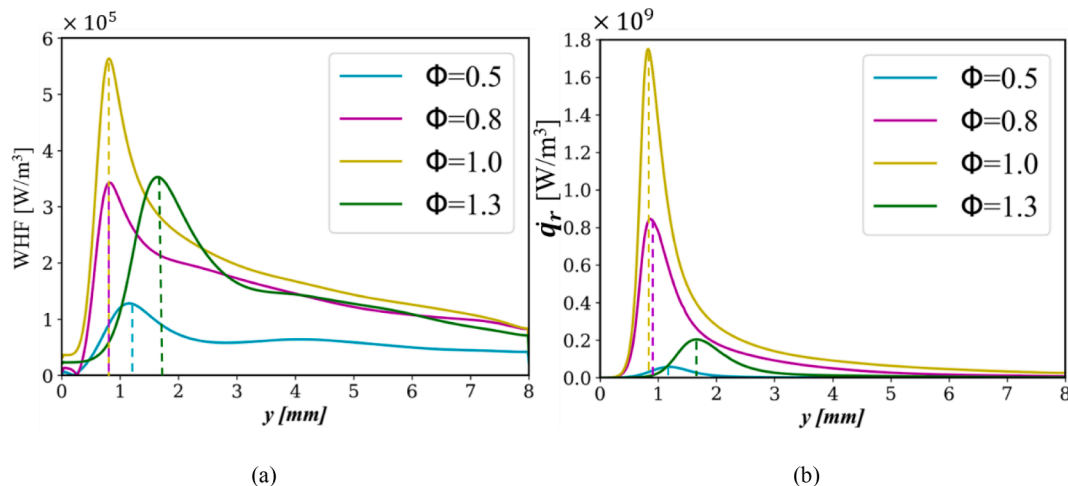


Fig. 5. Distribution of wall heat flux (left) and heat release rate (right) along the flame surface for different equivalence ratios.

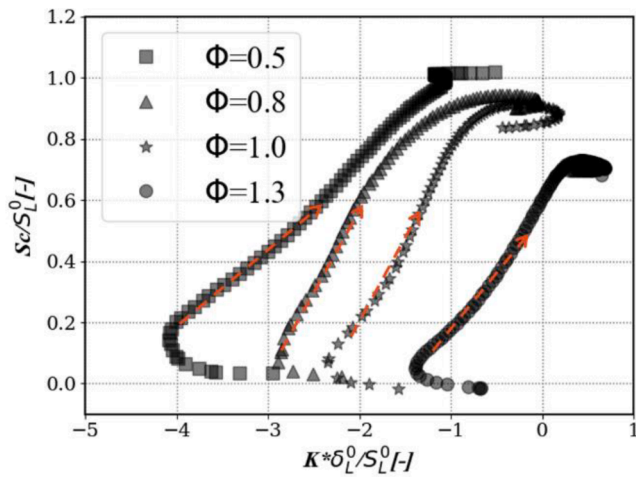


Fig. 6. Flame speed S_c versus normalized stretch rate Ka .

($T_w = T_u$), i.e., $WHF_{max} = 1/Pe_q$. The corresponding Pe_q at the various equivalence ratios are 0.92, 0.9, 0.87 and 1.14, respectively. According to Fourier's law, the temperature gradient near the wall is likewise the largest since the WHF_{max} at $\phi = 1.0$ is the largest, as shown in Fig. 5a. As a result, Pe_q at this condition is the smallest.

Fig. 6 depicts the correlation of flame consumption speed with the normalized stretch rate (Ka). Of particular interest is the response predicted by asymptotic theory indicating that the stretch forms a quasi-linear relationship with the flame speed under certain conditions, [38] given by:

$$\frac{S_c}{S_L^0} = 1 - \frac{L_a}{S_L^0} K \quad (1.8)$$

Table 2
Variation of d_q with ϕ for the different oscillating flames.

	$1/4f^{-1}$	$2/4f^{-1}$	$3/4f^{-1}$	Δd_q	Steady-state
d_q [mm]					
$\phi = 0.5$	0.28	0.34	0.75	0.47	0.44
$\phi = 1.0$	0.18	0.24	0.46	0.28	0.25
$\phi = 1.3$	0.37	0.45	0.54	0.17	0.36

Table 3
Variation of Pe_q with ϕ for the different oscillating flames.

	$1/4f^{-1}$	$2/4f^{-1}$	$3/4f^{-1}$	Steady-state
Pe_q				
$\phi = 0.5$	0.59	0.72	1.57	0.92
$\phi = 1.0$	0.63	0.83	1.60	0.87
$\phi = 1.3$	1.17	1.42	1.71	1.14

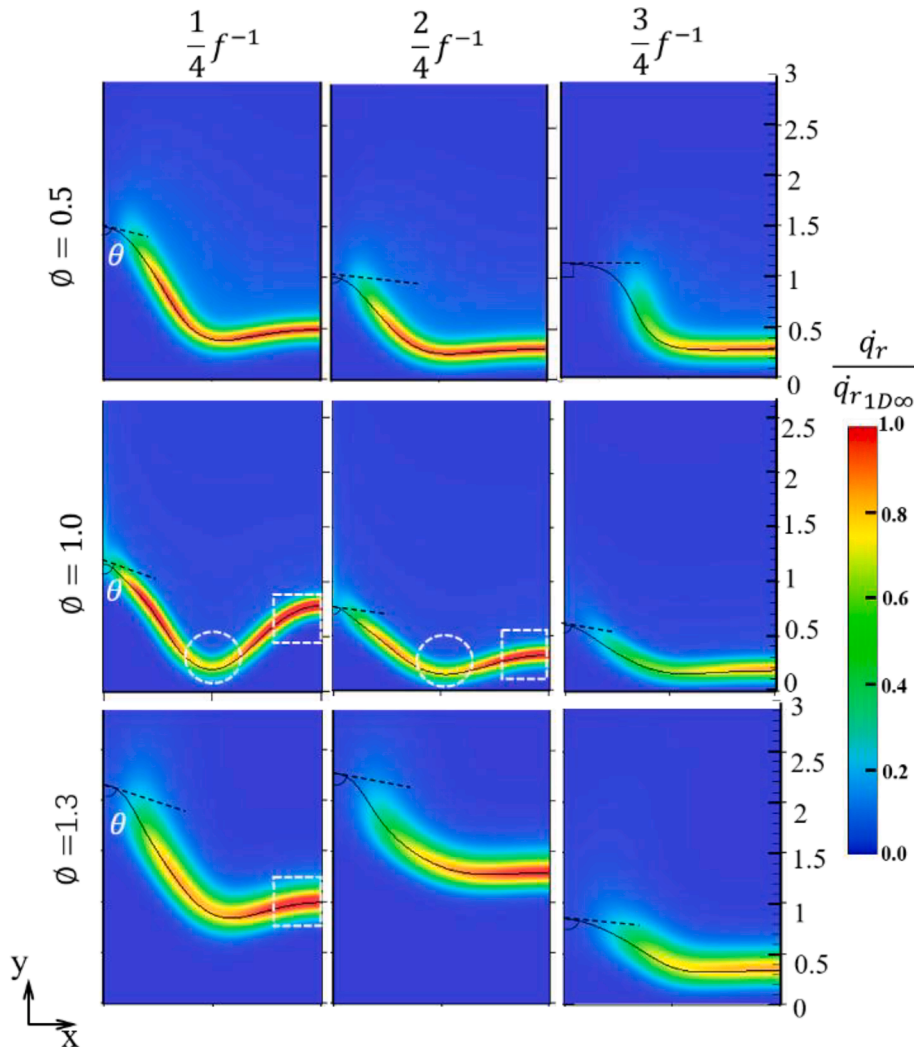


Fig. 7. Contours of flame surface and normalized heat release rate calculated from DNS of unsteady FWI at different phase angles during the oscillation.

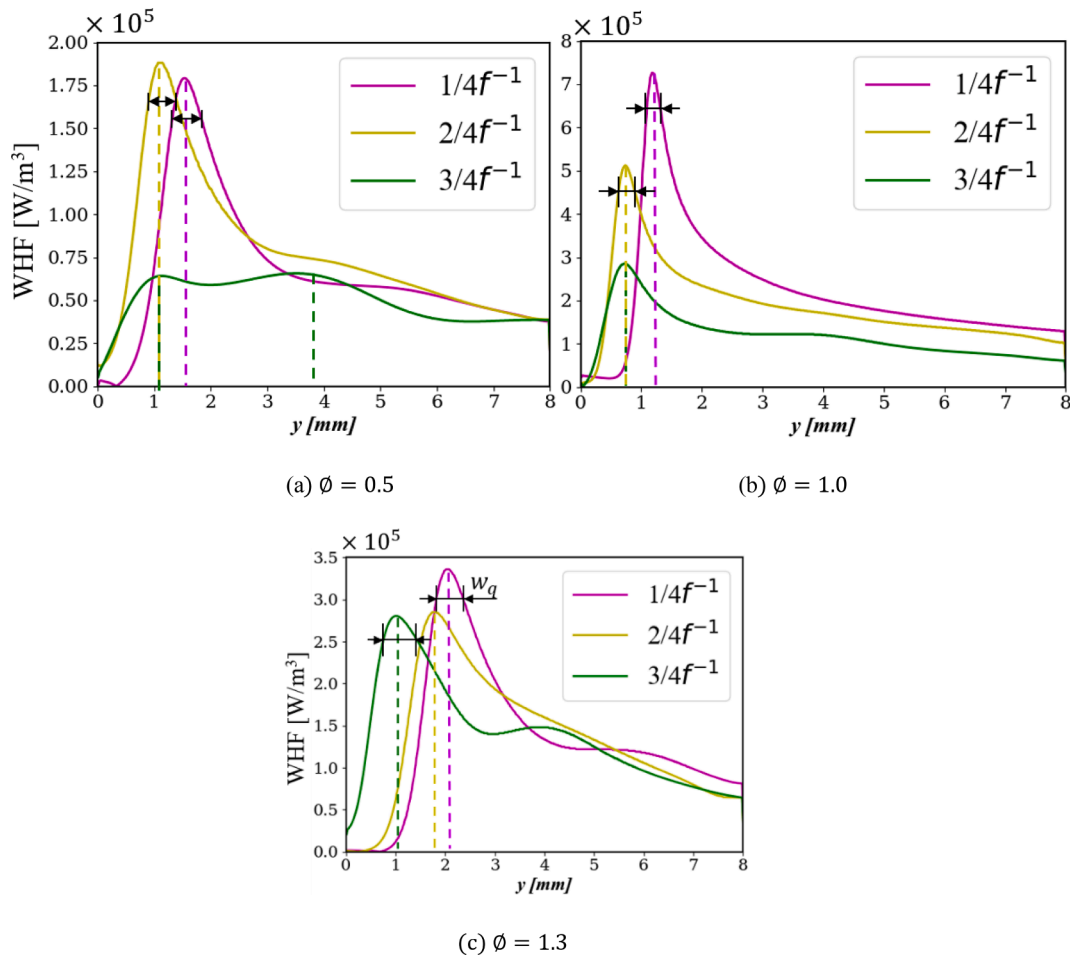


Fig. 8. Calculated heat flux at the wall from DNS of unsteady FWI.

$$\frac{S_c}{S_L^0} = 1 - Ma \frac{K\delta}{S_L^0} = 1 - MaKa \quad (1.9)$$

where L_a is the Markstein length and $Ma = \frac{dS_c/S_L^0}{dKa}$ the Markstein number, which is determined by fitting S_c/S_L^0 and Ka linearly. Ma can be used to determine how sensitive the flame speed is to flame stretch; Ma values for the various equivalence ratios mentioned above are -0.27 , -0.53 , -0.62 and -0.2 , respectively. Additionally, negative Ma only appear in the FWI zone and not for the free flame. A strong correlation between flame speed and flame stretch can be seen. However, there is non-linear relationship between the flame speed and flame stretch at the region very close to the wall, due to the heat losses. This results in a hook-shaped distribution with a lower flame speed at larger Ka .

4.2. Oscillating flames

According to the experiments of Jainki et al. [3], it has been found that the Helmholtz resonance frequency of the flame in a particular combustor is about 100 Hz, which leads to fluctuations in the flow direction at the flame tip. The magnitude of the fluctuation varies from combustor to combustor [4,28]. This section investigates how flames react dynamically to unsteady flow fields. Steady-state flames are influenced by the fluctuating flow at the inlet, and the functional expression for the inlet gas flow rate is $u_{in}(x,t) = u(x)(1 + a \sin(2\pi ft))$, where $u(x)$ denotes the parabolic velocity profile of the steady-state simulation, as shown in Fig. 2. The unsteady behavior of the inlet flow field is characterized by the excitation frequency (f) and amplitude (a). The relatively large a allows the flame fluctuations to be observed more

clearly. The excitation frequency $f = 100$ Hz and the relative amplitude $a = 0.6$ are used for the inflow velocity in this section, i.e., $u_{in}(x,t) = u(x)(1 + 0.6\sin(200\pi t))$.

Fig. 7 depicts the normalized heat release rate for the lean-premixed oscillating flame ($\phi = 0.5$), stoichiometric oscillating flame ($\phi = 1.0$) and rich oscillating flame ($\phi = 1.3$) at different instances within a forced cycle. The black solid line in the figure indicates the position of the flame surface. It is evident that the flame is affected by the inlet flow field during one oscillation cycle, causing the flame surface to oscillate significantly, changing the morphology of the flame. The flame height is at its maximum when the phase is at $1/4f^{-1}$. It then declines toward $2/4f^{-1}$ and reaches its minimum at $3/4f^{-1}$. Only phase angles from $1/4f^{-1}$ to $3/4f^{-1}$ are explored in this section since the flame at the initial phase angle of $0/4f^{-1}$ is almost the same as that at $2/4f^{-1}$. The angle (θ) between the tangential direction of the flame surface and the wall surface gradually increases until it reaches or approaches a straight angle as the flame propagates towards the inlet. At $3/4f^{-1}$, as the flame surface is close to the wall, the heat release rate is lower than it is at the other stages, while the stretch rate is larger than it is at the other stages (as shown in Fig. 10). At the same time, the mass flow of fresh fuel also declines, which causes a reduced fuel reaction rate and a positive stretch instead of a negative one. In addition, the heat release rate at $\phi = 1.0$ and $1/4f^{-1}$ is enhanced at the upward bend (depicted by the white square with dashed line) and weakened at the downward bend (marked by the white circle with dashed line). This is due to an imbalance between heat diffusion and mass diffusion that causes the flame to be extinguished. Although this phenomenon exists in the other two flames as well, it is most noticeable for $\phi = 1.0$.

Additionally, it has been demonstrated that the flame quenching

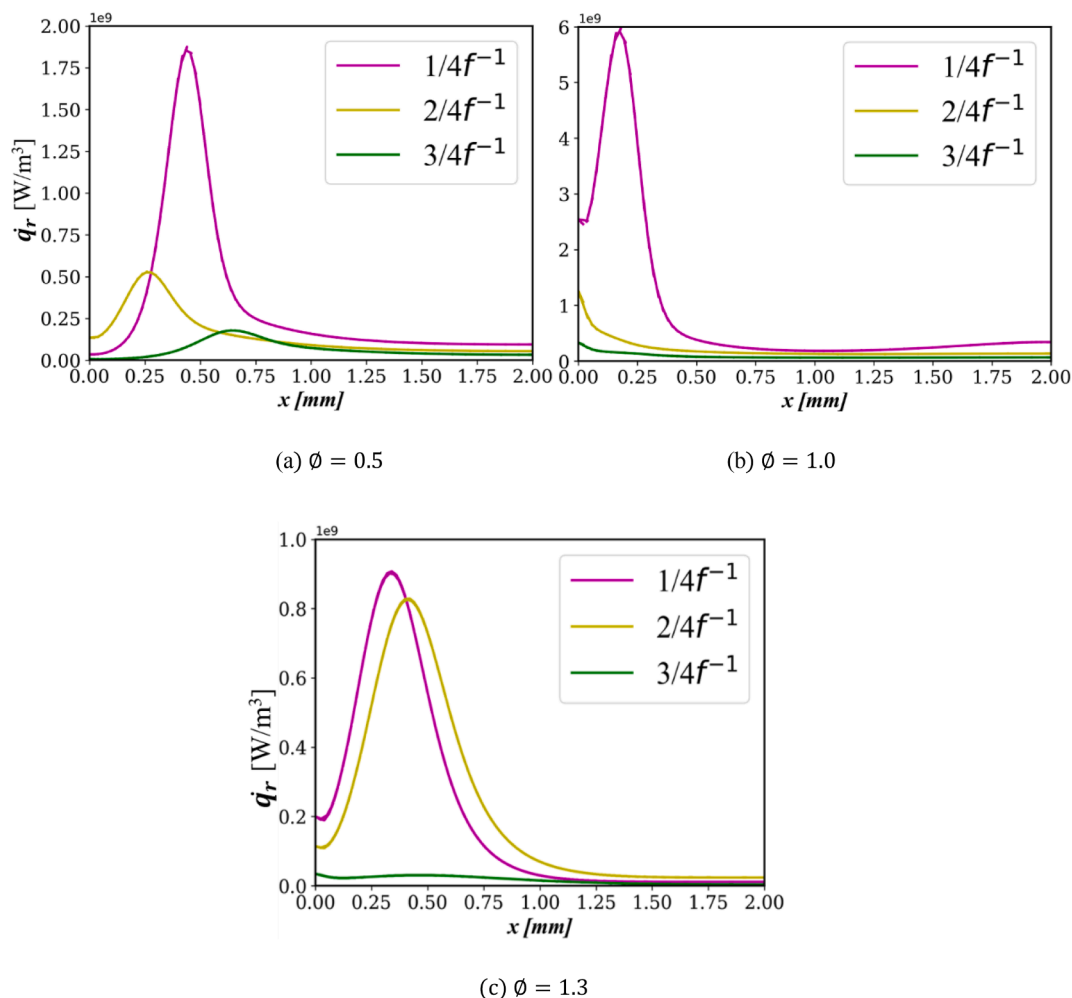


Fig. 9. Calculated heat release rate along the x-axis from DNS of unsteady FWI.

distance (d_q) is affected by the transient flow, but its variation is less than ± 0.05 mm [20]. Fig. 7 shows, in contrast, that the quenching distance d_q considerably fluctuates within the same cycle. In order to simplify the calculation of the quenching distance, the flame surface was determined using the aforementioned isotherm method. The quenching distances in one oscillation cycle and the variation of quenching distances were then compared under various equivalence ratios, as shown in Table 2. For different ϕ , d_q increases from $1/4f^{-1}$ to $3/4f^{-1}$ in one cycle during the oscillation. The difference between the maximum and minimum quenching distances, which decreases with increasing ϕ , is known as the quenching distance variation (Δd_q). For the same phase, d_q at $\phi = 1$ is smaller than that of other conditions. Moreover, d_q is similar to the experimental value of Jainki and Kosaka [4,39], whereas Δd_q is much larger than the results of Zirwes [20], which is due to the fact that the flame temperature is much larger than the wall temperature. Additionally, as the flame gets closer to the wall, the instantaneous wall heat flux is affected by the flame oscillation, which in turn leads to an increase in the variation of the quenching distance. The fact that a higher amplitude is used is possibly another important factor. Table 3 shows the trend of Pe_q with ϕ for different states. The trend is approximated by the quenching distance: for different equivalence ratios, Pe_q increases from $1/4f^{-1}$ to $3/4f^{-1}$ during the oscillation. Different from the trend of quenching distance, Pe_q gradually rises as ϕ rises.

In accordance with Fig. 7, the distribution of near-wall heat flux (WHF) along the y axis for different ϕ is shown in Fig. 8. At different time instances for the same mixture composition, the width (w_q) of the curve at the peak of WHF 10 % is nearly constant, but it differs

noticeably between different equivalence ratios. This is also present in the steady state, where at $\phi = 1$ it is the smallest and at $\phi = 1.3$ the largest. WHF is approximately 0 near the combustor entrance, increases sharply along the flow direction to a peak and then decreases slowly, and is significantly larger than 0 near the combustor exit. Additionally, throughout an oscillation cycle, the flame quenching point is continuously moving relative to the entrance. However, when $\phi = 0.5$ and the flame oscillates at $3/4f^{-1}$, the WHF has two peaks at the same time. This is because the flame is affected by the inlet velocity at that moment, causing the internal flow field to expand and the high-temperature zone to widen. This is followed by a slightly higher WHF at the outlet than the other instances. In addition, the maximum wall heat flux (WHF_{max}) corresponds to the y-axis positions of 1.1 mm, 1.2 mm, and 2.1 mm for the above conditions, respectively. The WHF also follows a similar trend as \dot{q}_r . The heat release rate variation along the wall-normal direction (x-axis) at these positions is extracted separately and shown in Fig. 9.

Previous studies have shown that the heat release rate increases significantly as the flame approaches the isothermal wall [9]. We set the wall temperature at 773 K for this paper. The heat release reaches its maximum at $\phi = 1.0$, $2/4f^{-1}$ and $3/4f^{-1}$. It is roughly 3.3 times greater than at $\phi = 0.5$ and 6.4 times greater than that at $\phi = 1.3$. At $\phi = 1.3$, there is more unburned fuel, which results in a slower effective heat release rate, and at $\phi = 0.5$ the heat generated by combustion is much lower than that at $\phi = 1.0$.

According to earlier studies [13], negative flame stretch dominates in the FWI region while it transitions from positive to negative for the free flame region. This phenomenon is similar to the trend of Ka along

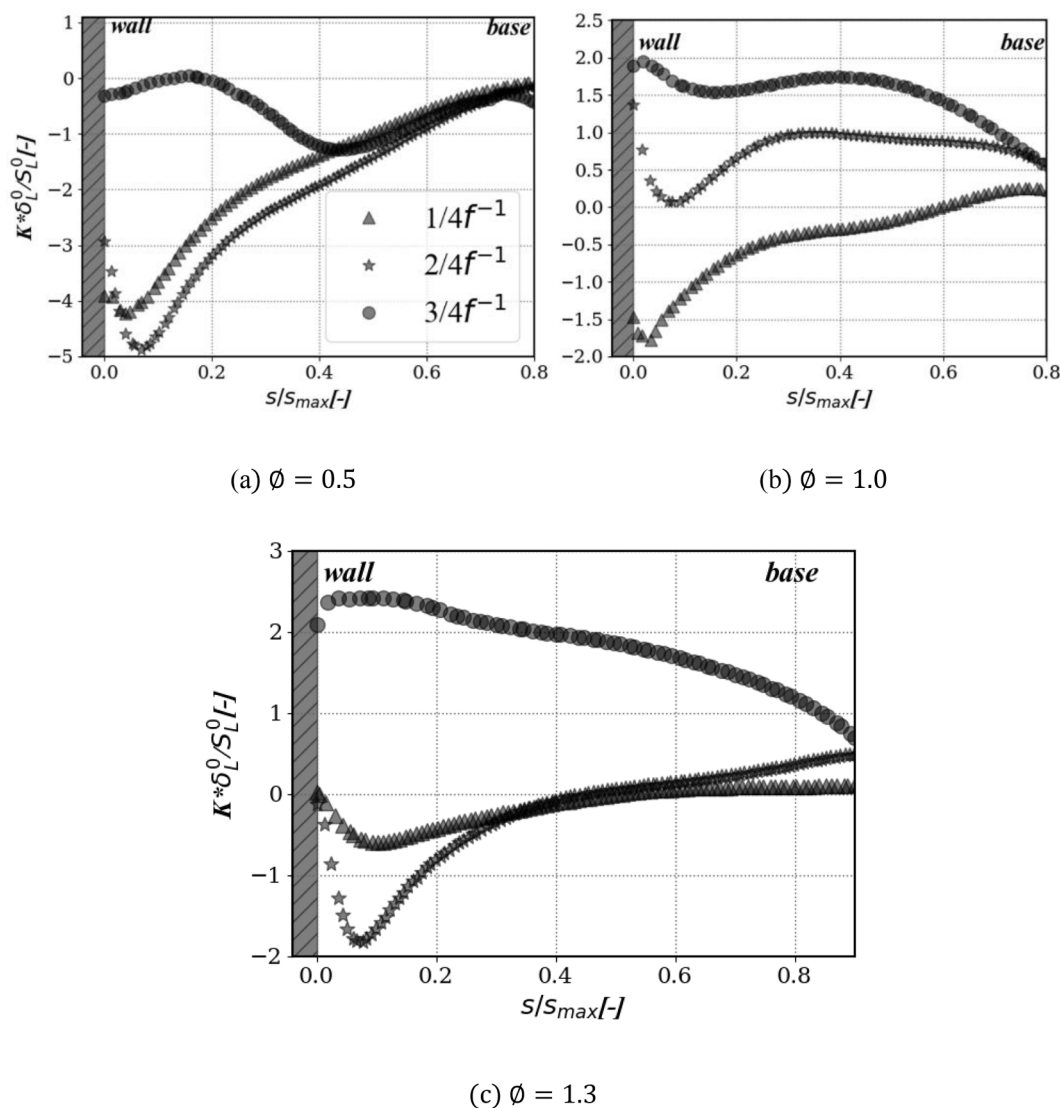


Fig. 10. Trends of stretch rate on the flame surface during unsteady FWI.

the flame surface, as depicted in Fig. 10. Ka is similar to the steady state at $1/4f^{-1}$ and $2/4f^{-1}$: negative stretch is formed near the wall, and the negative stretch rate is further reduced in a certain interval, while the Ka starts to increase after a certain distance from the wall and reaches a maximum at the base of the flame. Corresponding to Fig. 9, at position $x = 0.5$ mm at the top of the flame, where the heat release rate is likewise at a high value, the fuel reaction rate increases with rising Ka when $Le < 1$ and Ka is small [25]. The trend of the stretch rate changes from positive to negative tangential stretch at a phase angle of $3/4f^{-1}$, more closely resembling the stretch of a freely propagating flame. This is because the chemical reaction zone exits the wall-near region at that moment, causing WHF and \dot{q}_r to be lower than they would otherwise be.

Fig. 11 shows the relationship between the flame speed and the flame stretch along the flame surface for different phase angles within one oscillation period at different equivalence ratios. The strong association between flame speed and flame stretch during the flame oscillation cycle between $1/4f^{-1}$ and $2/4f^{-1}$ resembles the steady state. However, when the flame moves downstream, the flame speed at $3/4f^{-1}$ is significantly lower than it is at earlier stages because of the maximum fuel reaction rate at that moment, in accordance with Eq. (1.5), where S_c is negatively correlated with the fuel reaction rate. There is a negative slope at $3/4f^{-1}$, especially in Fig. 11(c), where the flame speed for the rich flame has a completely negative linear relationship with flame stretch. The specific

values are shown in Table 4. According to the variation of Ma with the phase angle at different equivalence ratios shown in Table 4, Ma fluctuates between positive and negative values. Combining the above information, it is reasonable to assume that Ma changes from negative to positive values when the effect of FWI is negligible or when the flame moves away from the wall. Furthermore, the flame stretches greatly while its speed increases nearly by a factor of two during the oscillation from phase angle $3/4f^{-1}$ to the next cycle $1/4f^{-1}$ at $\phi = 0.5$ and $\phi = 1.0$. This trend is also valid for methane/air flames for the range of 0.5 to 1.0.

5. Conclusions

In this work, the interaction of premixed methane/air flames with an isothermal wall at 773 K was simulated in order to evaluate the changing pattern of near-wall flame behavior. The detailed study of this phenomenon is both challenging computationally and experimentally, due to the generally small flame-wall interaction zone. Therefore, two-dimensional direct numerical simulations are performed for steady-state laminar flames and oscillating flames created by inflow fluctuations at different equivalence ratios. The objective is to analyze sidewall quenching when subjected to velocity perturbations at the entrance from both flame morphology and wall heat dissipation perspectives. While many studies exist that look at turbulent flame-wall interaction,

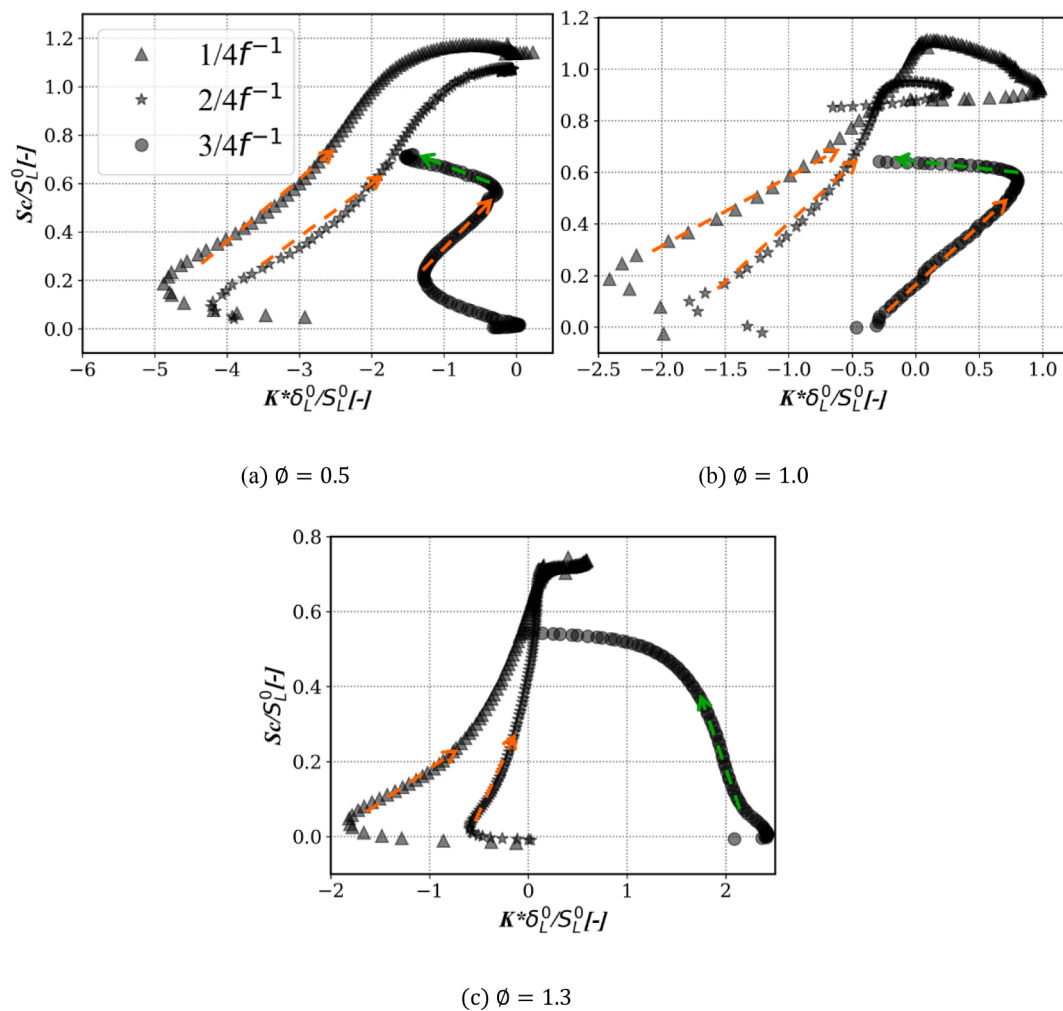


Fig. 11. Correlation of the flame speed with flame stretch during unsteady FWI.

Table 4
Variation of Ma with ϕ for the different oscillating flames.

		$1/4f^{-1}$	$2/4f^{-1}$	$3/4f^{-1}$	Steady-state
Ma	$\phi = 0.5$	-0.24	-0.26	0.11	-0.27
	$\phi = 1.0$	-0.26	-0.38	-0.44	-0.62
	$\phi = 1.3$	-0.16	-0.64	0.62	-0.2

much less work has been done to consider laminar flame-wall interaction cases with well-defined frequencies and amplitudes for the flame movement. The following findings have been presented in this work:

- (1) In the steady state, since WHF_{max} and Pe_q are inversely proportional, Pe_q is the smallest when WHF_{max} is the largest. Meanwhile at $\phi = 1.0$, Pe_q is the smallest among different equivalence ratios and WHF_{max} is the largest.
- (2) The heat loss of the flame to the wall modifies the local flame dynamics, leading to generally negative Markstein numbers while methane flames at the same condition without the influence of walls have generally positive Markstein numbers.
- (3) The Markstein numbers are additionally a function of the phase angle, when the flame oscillates due to forcing by the inflow. As the flame phase angle increases from $1/4f^{-1}$ to $3/4f^{-1}$, the stretch gradually changes from negative to positive for different equivalence ratios, and both the heat release rate along the flame surface and fuel reaction rate near the wall gradually decrease.

- (4) FWI is dominated by negative flame stretch, while positive flame stretch is present at the minimum flame height during the oscillation.
- (5) For equivalence ratios between 0.5 and 1.0, there is a nearly twofold increase in consumption speed during the oscillatory stretch of the methane/air flame. Additionally, when $\phi = 1.3$, the flame consumption speed is noticeably lower.
- (6) The general findings regarding the effect of oscillating flame-wall quenching scenarios are valid for both lean and rich methane/air flames.

The distinct impact of the time-dependent flame-wall interaction can be modeled by prescribing local Markstein numbers as a function of the distance and relative movement between the flame and the wall according to the presented findings.

CRedit authorship contribution statement

Jian Zhu: Conceptualization, Methodology, Validation, Formal analysis, Investigation, Data curation, Writing – original draft, Writing – review & editing. **Jianfeng Pan:** Resources, Writing – review & editing, Funding acquisition, Supervision. **Feichi Zhang:** Writing – review & editing. **Thorsten Zirwes:** Software, Writing – review & editing. **Abiodun Oluwaleke Ojo:** Writing – review & editing. **Feiyang Li:** Writing – review & editing.

Declaration of Competing Interest

The authors declare that they have no known competing financial interests or personal relationships that could have appeared to influence the work reported in this paper.

Data availability

The data that has been used is confidential.

Acknowledgements

This work was supported by the National Natural Science Foundation of China (Grant Nos. 51976082), Qing Lan Project, and Graduate Research and Innovation Projects of Jiangsu Province (KYCX18_2241).

References

- [1] Kim KT, Lee DH, Kwon S. Effects of thermal and chemical surface-flame interaction on flame quenching. *Combust Flame* 2006;146(1–2):19–28.
- [2] Fan Y, Suzuki Y, Kasagi N. Experimental study of micro-scale premixed flame in quartz channels. *Proc Combust Inst* 2009;32(2):3083–90.
- [3] Jaini C, Reißmann M, Böhm B, Dreizler A. Experimental investigation of flame surface density and mean reaction rate during flame-wall interaction. *Proc Combust Inst* 2017;36(2):1827–34.
- [4] Jaini C, Reißmann M, Böhm B, Janicka J, Dreizler A. Sidewall quenching of atmospheric laminar premixed flames studied by laser-based diagnostics. *Combust Flame* 2017;183:271–82.
- [5] Chen Y, Pan J, Lu Q, Wang Yu, Zhang C. Experimental investigation of flame structure and combustion limit during premixed methane/air jet flame and sidewall interaction. *Energy Eng* 2021;118(1):37–52.
- [6] Yang H, Feng Y, Wang X, Jiang L, Zhao D, Hayashi N, et al. OH-PLIF investigation of wall effects on the flame quenching in a slit burner. *Proc Combust Inst* 2013;34(2):3379–86.
- [7] De Lataillade A, Dabireau F, Cuenot B, Poinot T. Flame/wall interaction and maximum wall heat fluxes in diffusion burners. *Proc Combust Inst* 2002;29(1):775–9.
- [8] Popp P, Baum M. Analysis of wall heat fluxes, reaction mechanisms, and unburnt hydrocarbons during the head-on quenching of a laminar methane flame. *Combust Flame* 1997;108(3):327–48.
- [9] Dabireau F, Cuenot B, Vermorel O, Poinot T. Interaction of flames of H₂ + O₂ with inert walls. *Combust Flame* 2003;135(1–2):123–33.
- [10] Yenerdag B, Minamoto Y, Aoki K, Shimura M, Nada Y, Tanahashi M. Flame-wall interactions of lean premixed flames under elevated, rising pressure conditions. *Fuel* 2017;189:8–14.
- [11] Strassacker C, Bykov V, Maas U. REDIM reduced modeling of quenching at a cold wall including heterogeneous wall reactions. *Int J Heat Fluid Flow* 2018;69:185–93.
- [12] Jafargholi M, Giannakopoulos GK, Frouzakis CE, Boulouchos K. Laminar syngas-air premixed flames in a closed rectangular domain: DNS of flame propagation and flame/wall interactions. *Combust Flame* 2018;188:453–68.
- [13] Law CK. *Combustion physics*. Cambridge University Press; 2006.
- [14] Creta F, Matalon M. Strain rate effects on the nonlinear development of hydrodynamically unstable flames. *Proc Combust Inst* 2011;33(1):1087–94.
- [15] Liang W, Wu F, Law CK. Extrapolation of laminar flame speeds from stretched flames: Role of finite flame thickness. *Proc Combust Inst* 2017;36(1):1137–43.
- [16] Giannakopoulos GK, Frouzakis CE, Mohan S, Tomboulides AG, Matalon M. Consumption and displacement speeds of stretched premixed flames - Theory and simulations. *Combust Flame* 2019;208:164–81.
- [17] Zhang F, Zirwes T, Häber T, Bockhorn H, Trimis D, Suntz R. Near wall dynamics of premixed flames. *Proc Combust Inst* 2021;38(2):1955–64.
- [18] Zhang F, Zirwes T, Habisreuther P, Bockhorn H. Effect of unsteady stretching on the flame local dynamics. *Combust Flame* 2017;175:170–9.
- [19] Chen JB, Hong GI. Stretch effects on the burning velocity of turbulent premixed hydrogen/air flames. *Proc Combust Inst* 2000;28(1):211–8.
- [20] Zirwes T, Häber T, Zhang F, Kosaka H, Dreizler A, Steinhausen M, et al. Numerical study of quenching distances for side-wall quenching using detailed diffusion and chemistry. *Appl Sci Res* 2021;106(2):649–79.
- [21] Palulli R, Talei M, Gordon RL. Unsteady flame-wall interaction: Impact on CO emission and wall heat flux. *Combust Flame* 2019;207:406–16.
- [22] Karlovitz B, Denniston DW, Knapschafer DH, Wells FE. *Studies on Turbulent flames*. Symp (Int) Combust 1953;4(1):613–20.
- [23] Williams F A. *Combustion theory. Fundamental theory of chemically reacting flow systems*, 1985, 3:215–228.
- [24] Lipatnikov. *Fundamentals of premixed turbulent combustion*. Taylor & Francis; 2013.
- [25] Poinot T, Veynante D. *Theoretical and numerical combustion*. RT Edwards, Inc., 2005.
- [26] Zhang FC, Bonart H, Zirwes T, et al. Direct numerical simulation of chemically reacting flows with the public domain code OpenFOAM. Springer International Publishing; 2015.
- [27] White F, Ng C, Saimek S. *Fluid Mechanics* (7th ed.). McGraw-Hill, cop. 2011.
- [28] Häber T, Suntz R. Effect of different wall materials and thermal-barrier coatings on the flame-wall interaction of laminar premixed methane and propane flames. *Int J Heat Fluid Flow* 2018;69:95–105.
- [29] Zirwes T, Zhang F, Denev J A, et al. Automated code generation for maximizing performance of detailed chemistry calculations in OpenFOAM. *High Performance Computing in Science and Engineering*, 2018: 10.1007/978-3-319-68394-2_11.
- [30] Zirwes T, Zhang F, Denev JA, et al. Improved vectorization for efficient chemistry computations in OpenFOAM for large scale combustion simulations. Springer International Publishing; 2019. p. 209.
- [31] Zirwes T, Zhang F, Habisreuther P, Hansinger M, Bockhorn H, Pfitzner M, et al. Quasi-DNS dataset of a piloted flame with inhomogeneous inlet conditions. *Flow, Turbulence Comb* 2020;104(4):997–1027.
- [32] OpenFOAM: The open source CFD toolbox. www.openfoam.com.
- [33] Weller HG, Tabor G, Jasak H, Fureby C. A tensorial approach to computational continuum mechanics using object-oriented techniques. *Comp Phys* 1998;12(6):620–31.
- [34] Goodwin DG, Moffat HK, Speth RL. Cantera: An object-oriented software toolkit for chemical kinetics, thermodynamics, and transport processes. <http://www.cantera.org>. 2016. Version 2.2.1.
- [35] Poinot T, Haworth D, Bruneaux G. Direct simulation and modeling of flame-wall interaction for premixed turbulent combustion. *Combust Flame* 1993;95(1–2):118–32.
- [36] Bush WB. Asymptotic analysis of laminar flame propagation: review and extension. *Int J Eng Sci* 1979;17(5):597–613.
- [37] Kosaka H, Zentgraf F, Scholtissek A, Bischoff L, Häber T, Suntz R, et al. Wall heat fluxes and co formation/oxidation during laminar and turbulent side-wall quenching of methane and DME flames. *Int J Heat Fluid Flow* 2018;70:181–92.

Further reading

- [35] SUNDIALS: Suite of nonlinear and differential/algebraic equation solvers. <http://computation.llnl.gov/case/sundials/main.html>.
- [36] Lieuwen TC, Murray NE. Unsteady combustor physics. *J Acoust Soc Am* 2013;134(2):1431.